Springer

Journal of Mechanical Science and Technology 22 (2008) 2048~2055

Journal of Mechanical Science and Technology

www.springerlink.com/content/1738-494x
DOI 10.1007/s12206-008-0806-x

Intrinsic stress, mismatch strain, and self-assembly during deposition of thin films subjected to an externally applied force †

Sang-Hyun Kim[1,*] and James G. Boyd IV[2]

[1]*Mechanical Systems Engineering, Hansung University, Samseon-dong 3-ga, Seongbuk-gu, Seoul, 136-792, Korea,*
[2]*Department of Aerospace Engineering, 3141 TAMU, Texas A&M University, College Station, TX, 77843-3141, USA*

(Manuscript Received February 13, 2008; Revised July 18, 2008; Accepted August 4, 2008)

Abstract

A relation is derived between the mismatch strain, the film thickness, and the displacement of a linear elastic structure under external loading during material deposition. If any two of these variables can be experimentally determined, then the remaining variable can be determined. The method allows one to experimentally determine the mismatch strain by measuring the film thickness and the displacement of a point on the structure that is not undergoing deposition. The intrinsic stresses can be used to self-assemble microstructures during material deposition. Assembly of two components is considered: one component is subjected to deposition and is modeled as an Euler-Bernoulli beam, and the other component is not subjected to deposition and is modeled as a linear spring. For the purposes of this paper, the definition of assembly requires that the beam do work on the spring. The analysis is experimentally verified by electroplating nickel onto an AFM cantilever beam in contact with a second AFM beam (serving as the spring) that does not undergo deposition.

Keywords: Intrinsic stress; Mismatch strain; Self-Assembly; Electroplated nickel; Electrodeposition

1. Introduction

Intrinsic stresses result from lattice mismatch and/or growth processes during chemical vapor deposition, physical vapor deposition, and electrodeposition. Intrinsic stresses are usually deleterious in thin films and often result in warping, buckling, blistering, cracking, delamination, and void formation. Intrinsic stresses are also called residual stresses because they exist in the absence of an applied load.

The research reported herein extends the state of the art in two subjects related to intrinsic stresses in thin films. First, intrinsic stresses are usually measured when material is deposited uniformly in the plane of the wafer. However, the fabrication of micro electromechanical systems (MEMS) and nano electromechanical systems (NEMS) often involves deposition onto a region that is in contact with another region that does not undergo deposition. For example, electrodeposition is often performed on a patterned seed layer. The method reported herein enables device engineers to measure the intrinsic stress in the deposited region by measuring a displacement in the non-deposited region.

Second, the method reported herein advances the subject of using intrinsic stresses for self-assembly. Many researchers have used intrinsic stresses advantageously to bend plates or beams in the out-of-plane direction during processing. A common procedure is to deposit at least two layers and then remove a lower sacrificial layer, enabling the upper layers to deform. Ataka et al. [1] made a thermal bimorph cantilevered beam from polyimide that curled up above the substrate after the sacrificial layer was removed. During subsequent operation, heating of a metallic layer bent

† This paper was recommended for publication in revised form by Associate Editor Maenghyo Cho

*Corresponding author. Tel.: +82 2 760 8012, Fax.: +82 2 760 4329
E-mail address: shkim@hansung.ac.kr

the beam towards the substrate. Ho et al. [2] used a MUMPS-like process with low-stress "SixNy" and polysilicon in which residual stresses created a pop-up mirror. Xie et al. [3] used residual stresses to make a rotational electrostatic comb drive. Capacitor fingers of one polarity were made in the traditional fixed manner, and fingers of the opposite polarity were connected to beam hinges made by depositing aluminum on silicon oxide. When the oxide was etched away, the aluminum beams rotated out-of-plane due to residual stresses. Thus, when a potential difference was applied to the two capacitor fingers, the movable finger achieved a rotation of up to 4.7° toward the substrate. Prinz et al. [4] used residual stresses to make cylindrical nano structures. A laminate consisting of B doped Si, undoped Si, B doped Si, Ge, and B doped Si was deposited with no curvature. The undoped Si layer was etched away, allowing the upper three layers (B doped Si, Ge, B doped Si) to roll up into cylinders with radii of curvature from 0.3 to 2 micrometers. Mi et al. [5] used residual stresses to control the curvature of a micromirror. Layers of polysilicon and silicon dioxide were deposited with no curvature by using LPCVD, and when the oxide was etched away, the polysilicon was deformed into a curved structure with a radius of curvature of 6.4mm. In a series of papers, Vacarro, Kubota and coworkers [6-8] made a standing mirror using lattice-mismatched epitaxial layers from a multilayer plate including AlGaAs/GaAs dielectric mirror and InGaAs strained layer grown on a GaAs substrate. The plate bent out-of-plane after the sacrificial layer was removed. They also allowed a SiGe/Si bilayer to curl up into tubes and spirals by removing a SiO2 layer [9]. The previously mentioned studies rotated a structure about an axis in the plane. In contrast, Judy et al. [10] rotated a polysilicon/silicon nitride beam about an axis out-of-plane. The beam rotated laterally when the sacrificial oxide layer was etched away. In all of these studies, the moving part was free from external loads.

In the present paper we analyze the mechanics of assembling two components due to deposition of one component. Suppose that two components are to be assembled by deposition of one component. The component being deposited must do work on the other component. Thus, the component being deposited is subject to an external load in addition to residual stress. The component subject to deposition is modeled as an Euler-Bernoulli composite beam (Fig. 1). The other component is modeled as a linear spring of stiffness K_S. For the purposes of this paper, the definition of assembly requires that the beam do work on the spring. Thus, the component being deposited is subject to an external load from the spring. Such an assembly could be used to lock two parts together, make an electrical contact between two or more parts, close an open volume, insert a dielectric material between two conductors, or apply a preload to a spring.

Much research has been done to analyze the stress and deformation in thin films due to intrinsic stresses. This work dates to the Stoney formula [11] for the curvature of thin films on a thick substrate. Freund [12] extended Stoney's work to include the dependence of the mismatch strain on the local deposition conditions, for example, when the magnitude of the mismatch strain depends on the state of strain, and hence curvature, of the deposition surface. For layered microstructures, Ni et al. [13] provided an experimentally verified method to predict the intrinsic stress distribution before release and the curvature after release. The analysis was based on a lamination theory in which the mismatch strain could vary across the thickness of each layer. Thus, Ni et al. provided a systematic way of designing the structures made by researchers in references [1-10]. However, these previous studies did not include the effects of externally applied loads during deposition.

The outline of the present paper is as follows. The model and analytical results are presented in Section 2. An experimental verification of the analysis is presented in Section 3. The emphasis herein is on the analytical method, not a specific device. The method can easily be extended to other geometries and loads, such as plates or shells loaded by distributed forces or moments.

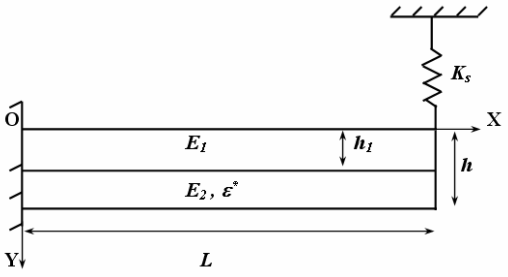

Fig. 1. An Euler-Bernoulli composite beam connected to a linear spring.

2. Deposition model

The prismatic beam has constant length L, constant width b, and variable thickness h. The substrate with Young's modulus of E_1 is designated as region 1 and has a constant thickness h_1. The deposited material with Young's modulus of E_2 has a variable thickness h_2, and $h = h_1 + h_2$. The spring represents the elastic deformation of the region of the MEMS or NEMS device that does not undergo deposition. The spring is attached to the center of the end of the beam [$(x, y, z) = (L, 0, 0)$] when $h = h_1$ in such a way that there is initially no load on the spring or beam. Material is then deposited on the surface $y = h$ $(h \geq h_1)$, which causes the beam to bend and the spring to either compress or stretch, depending on the sign of the mismatch strain in the deposited material. Kim and Boyd [14, 15] investigated the mechanical behavior of a multilayered microcantilever with the through-thickness variation of mismatch strain during the deposition process. Referring to the results of Kim and Boyd [14, 15], the moment increment of microcantilever is expressed in terms of the curvature increment and the thickness increment,

$$\frac{dM\{x;h\}}{bE_1} = \frac{1}{12\bar{E}} f\{h\} d\kappa\{x;h\} + \frac{\varepsilon^*\{h\}}{2\bar{E}} g\{h\} dh \quad (1)$$

where $\bar{E} = E_1 / E_2$ and

$$f\{h\} = \left(h + (\bar{E}-1)h_1\right)^{-1}\left(-h^4 - 4h^3 h_1(\bar{E}-1) + 6h^2 h_1^2(\bar{E}-1) - 4hh_1^3(\bar{E}-1) - h_1^4(\bar{E}-1)^2\right)$$

$$g\{h\} = \left(h + (\bar{E}-1)h_1\right)^{-1}\left(h^2 + 2hh_1(\bar{E}-1) - h_1^2(\bar{E}-1)\right)$$

For a spring attached to the beam the increment of moment is non-zero and is given by

$$dM\{x;h\} = dP\{h\}(x - L) \quad (2)$$

where $dP\{h\}$ is the increment of load applied to the beam at $x = L$ by the spring. To determine the beam deflection it is necessary to introduce the approximate increment of curvature as

$$d\kappa\{x;h\} = \frac{d^2}{dx^2} dv\{x;h\} \quad (3)$$

where $v\{x;h\}$ is the displacement of the beam in the y direction. Eqs. (2) and (3) can be substituted into Eq. (1), together with the boundary conditions $0 = v\{0;h\} = \frac{d}{dx} v\{0;h\}$ to yield

$$\frac{dP\{h\}}{bE_1}\left(\frac{1}{6}x^3 - \frac{1}{2}Lx^2\right) = \frac{f\{h\}}{12\bar{E}} dv\{x;h\} + \frac{\varepsilon^*\{h\}}{4\bar{E}} x^2 g\{h\} dh \quad (4)$$

We can now introduce the relationship between the load increment on the beam and the increment of deflection of the spring:

$$dP\{h\} = -K_s dv\{L;h\} \quad (5)$$

Eq. (5) can be substituted into Eq. (4) to obtain an ordinary linear differential equation for $v\{L;h\}$ as a function of h:

$$\frac{dv\{L;h\}}{dh} = \left(\frac{K_s L^3}{3bE_1} - \frac{f\{h\}}{12\bar{E}}\right)^{-1} \frac{\varepsilon^*\{h\} L^2 g\{h\}}{4\bar{E}} \quad (6)$$

Eq. (6) provides a relationship between the mismatch strain, the film thickness, and the deflection of a linear elastic structure under external loading during material deposition. If any two of these variables can be experimentally determined, then the remaining variable can be determined. If $\varepsilon^*\{y\}$ is known, then Eq. (6) can be solved for $v\{L;h\}$ as a function of h. Therefore, if one can measure h, then $v\{L;h\}$ is experimentally determined. Alternatively, if one can measure $v\{L;h\}$, then h is experimentally determined. If h and $v\{L;h\}$ can be measured, then $\varepsilon^*\{y\}$ can be experimentally determined. Recall that the spring represents a linear elastic region (or structure) that is not undergoing deposition. If one can measure the displacement of any point on this 'spring" structure, then linear elasticity can be used to determine $v\{L;h\}$. For linear elastic structures, this method can easily be extended to geometries other than beams, such as plates, shells, etc. Although the method is complicated by the need to solve a linear elastic boundary value problem, closed-form solutions are available for many common geometries. For more complicated geometries with linear problems, finite element codes can provide easy and accurate solutions.

3. Deposition experiment

3.1 Experimental overview

The goal of the experiment is to physically realize the device of Fig. 2 and measure the variables that are required to verify the deposition model. The device will consist of two cantilevered AFM beams in contact at their ends, as shown in Fig. 2. Material is electroplated onto the lower side of the "deposition" beam (the beam on the left), which produces residual stresses that deform the beam. The deposition beam is in unbonded contact with a "spring" beam (the beam on the right) that is not electroplated. As the deposition beam deforms, it does work on the spring beam. The deposition beam also serves as the sensing beam because its end deflection is optically measured on the upper surface by using an atomic force microscope (AFM). The beams are supplied with a 10nm silicon nitride passivation layer applied to both sides of the beams. A Cr/Au seed layer is then evaporated onto the lower side of the deposition beam to provide electrical conductivity for subsequent electroplating of nickel. The following variables must be measured: the stiffness of the spring beam, the dimensions of the deposition beam, the thickness of the various layers that constitute the deposition beam, the Young's modulus of the deposited nickel, and the end deflection of the deposition beam as a function of the deposition thickness when the deposition beam is both attached and unattached to the spring beam.

The AFM beams (MikroMasch, USA, $NSC16/Si_3N_4$) have a trapezoidal cross section with a wide side to reflect the laser light. The beam width is usually given as the average of the two sides of the trapezoid. The nominal beam dimensions are $230\ \mu m\times$, $40\ \mu m\times 7.0\ \mu m$ the nominal spring constant is 40 N/m, and the nominal resonant frequency is 170 kHz. The deposition cantilever is the working electrode and an insoluble anode (platinum wire, Model CHI115 from CH Instruments, Inc.) is used as the counter electrode. A nanoscope IIIA AFM (Digital Instruments, Inc.) is used with an electrochemical cell (Fluid Image Cell & Accessory Kit from Digital Instruments, Inc.). The electrochemical cell encloses the working and counter electrodes.

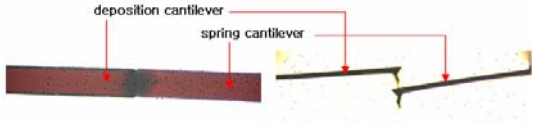

(a) (b)

Fig. 2. Images of aligned cantilevers (a) top view (b) side view.

3.2 Finding the reference mismatch strain

In order to numerically solve Eq. (6), the reference mismatch strain $\varepsilon^*\{y\}$ must be known. The reference mismatch strain will be determined by interpreting experimental results in terms of the relation between the beam curvature and the mismatch strain. The mismatch strain is simply expressed by

$$\varepsilon^m\{y\}=\varepsilon^*\{y\}+y\kappa\{x;y\}-\varepsilon^r\{y\} \tag{7}$$

where $\kappa\{x;y\}$ is the curvature about the z axis and $\varepsilon^r\{y\}$ is the strain of the reference layer, $y=0$. The curvature and the reference strain can be written in terms of the mismatch strain as,

$$\kappa\{x;h\}=-\frac{6}{h^2}\frac{A\{h\}}{D\{h\}}\int_0^h\varepsilon^m\{y\}dy+\frac{12}{h^3}\frac{B\{h\}}{D\{h\}}\int_0^h y\varepsilon^m\{y\}dy \tag{8}$$

$$\varepsilon^r\{x;h\}=-\frac{4}{h}\frac{C\{h\}}{D\{h\}}\int_0^h\varepsilon^m\{y\}dy+\frac{6}{h^2}\frac{A\{h\}}{D\{h\}}\int_0^h y\varepsilon^m\{y\}dy \tag{9}$$

where,

$$A\{h\}=\frac{h_1^2}{h^2}(\bar{E}-1)+1, B\{h\}=\frac{h_1}{h}(\bar{E}-1)+1, C\{h\}=\frac{h_1^3}{h^3}(\bar{E}-1)+1,$$

$$D\{h\}=4\left[\frac{h_1}{h}(\bar{E}-1)+1\right]\left[\frac{h_1^3}{h^3}(\bar{E}-1)+1\right]-3\left[\frac{h_1^2}{h^2}(\bar{E}-1)+1\right]^2$$

Substituting Eqs. (8) and (9) into Eq. (7) yields:

$$\varepsilon^*\{y\}=\varepsilon^m\{y\}-\frac{2}{yD\{y\}}\left[2C\{y\}-3A\{y\}\right]\int_0^y\varepsilon^m\{y\}dy-\frac{6}{y^2D\{y\}}\left[2B\{y\}-A\{y\}\right]\int_0^y y\varepsilon^m\{y\}dy \tag{10}$$

Therefore, the reference mismatch strain $\varepsilon^*\{y\}$ can be determined if the mismatch strain $\varepsilon^m\{y\}$ is obtained. This mismatch strain can be obtained through the experiment results. $\varepsilon^m\{y\}$ can be obtained from experiment results. In the first experiment reported herein, $v\{L;h\}$ is measured as a function of h when no spring is attached. The approximate increment of curvature is given by

$$d\kappa\{x;h\} = \frac{d^2}{dx^2} dv\{x;h\} \tag{11}$$

In this particular case, $\kappa\{x;h\} = \kappa\{h\}$ because κ is not a function of x because there is no external load (no spring to load the beam) and it is assumed that the deposited layer is applied in a manner that is not a function of x. Integrating Eq. (11) twice with respect to x and using the boundary conditions $0 = v\{0;h\} = \frac{d}{dx} v\{0;h\}$ results in

$$\kappa\{h\} = \frac{2v\{L;h\}}{L^2} \tag{12}$$

when x is evaluated at L. From Eq. (12), for each value of h, the curvature can be experimentally obtained from the beam end deflection. The out-of-plane variation of the mismatch strain $\varepsilon^m\{y\}$ can be approximated as a polynomial function of y

$$\varepsilon^m\{y\} = a + by + cy^2 + dy^3 + ey^4 \cdots \tag{13}$$

and the unknown parameters (a,b,c, . . .) can be determined from Eq. (8). Finally, the reference mismatch strain $\varepsilon^*\{y\}$ can be determined from Eq. (10).

3.3 Experimental procedure

The beam dimensions were measured with a scanning electron microscope. A Cr/Au seed layer of nominal thickness $(Cr: 5\ nm,\ Au: 50\ nm)$ was evaporated onto the bottom side of the deposition cantilever. The film thicknesses were measured by using a stylus profilometer (DEKTAK). Sader's method [16] was used to determine the spring constant (stiffness) of the cantilever beam in the liquid cell as

$$k = 0.1906 \rho_f b^2 L Q_f \Gamma_i(\omega_f) \omega_f^2 \tag{14}$$

ρ_f is the mass density of the fluid, b and L are the thickness and length of the beam, Q_f and ω_f are the quality factor and the beam resonant frequency in fluid, and Γ_i is the imaginary part of the hydrodynamic function, which depends only on the Reynolds number.

Young's modulus of electroplated nickel varies greatly depending on the processing conditions [17]. Therefore, rather than use a published value for Young's modulus, it was experimentally obtained from the spring constant k of the composite cantilever beam from elementary beam theory:

$$k = \frac{3b}{L^3} \sum_i E_i \left(\frac{h_i^3}{12} + h_i (z_i - z_n)^2 \right) \tag{15}$$

where E_i is Young's modulus of the i^{th} layer, z_i and z_N are the distances from the bottom of the beam to the center of the i^{th} layer and the neutral axis, and h_i is the thickness of the i^{th} layer. The spring constant, the deposited film thickness and the beam dimensions were measured. Therefore, Young's modulus of the electroplated nickel can be determined.

The beam deflection cannot be measured directly as a function of the deposited layer thickness during electroplating. Instead, the nickel plating rate is measured by plating in a series of steps and using the profilometer to measure the nickel thickness after each plating step. Then the deflection of the deposition beam is measured as a function of time when the deposition beam is not in contact with the spring beam. Since both the deflection and the deposition thickness are known functions of time, it is possible to express the beam deflection as a function of the deposited film thickness. The deflections can then be converted into curvatures by using Eq. (12). Finally, the reference mismatch strain as a function of the out-of-plane coordinate is calculated from Eq. (10).

Intrinsic stresses in electrodeposited nickel can vary greatly depending on the solution composition and operating conditions [18]. In general, electrodeposited nickel exhibits a tensile intrinsic stress between 125 to 185 MPa for additive-free Watts solutions, 0 to 55 MPa for nickel sulfamate solutions, and 120 MPa all-sulfate solutions. An all-sulfate nickel solution is used herein. The basic constituents for all-sulfate solution include 225~410 g/L of nickel sulfate ($NiSO_4 \cdot 6H_2O$) as the primary source of nickel ions and 30~45 g/L of boric acid (H_3BO_3) to stabilize the pH of the solution. Nickel carbonate ($NiCO_3$) can be added to control the pH

and maintain the nickel ion concentration. In order to obtain a high residual stress, the pH was maintained greater than 4.

The two beams were aligned and placed in contact at their ends by using two orthogonally arranged optical microscopes and precision positioners. The two beams were held in this arrangement by bonding their cantilever chips (the large substrate to which the beams are attached) to a common "cross bar" that does not contact the beams.

3.4 Experimental results and discussion

The variation in stiffness among the beams is unimportant because the stiffness of each beam is measured individually. However, it is important to verify that the elementary beam theory is adequate for beam analysis. Therefore, the stiffness of nine "spring" beams (Fig. 2(b)) was experimentally determined, with an average stiffness of 38.7 N/m and a standard deviation of 2.27 N/m. The beam stiffnesses were also calculated with elementary beam theory by using the measured dimensions and published values for Young's modulus of silicon and silicon nitride. The average calculated stiffness and standard deviation for the nine beams were 39.2 N/m and 2.30 N/m, demonstrating excellent agreement between the experimental and analytical values of the beam stiffness.

Young's modulus of electroplated nickel was determined for each of five plating time steps for four beams; it ranged between 163 GPa and 176 GPa, with an average of 171 GPa.

The experimentally measured plating rate was determined by using four beams and measuring the plating thickness at the end of each of five fifteen second plating steps. The plating rates differed by a maximum of 8%. The average experimentally measured plating rate differed from the analytically predicted rate by less than 0.5%.

In order to determine the reference mismatch strain, nickel was electroplated onto one side of six beams that were not attached to a "spring" beam. The beam deflections were determined as a function of plating thickness, and then the deflections were converted into curvatures by using Eq. (12). Finally, the reference mismatch strain as a function of the out-of-plane coordinate was calculated for six beams, and the average response is shown in Fig. 3.

The end deflection of the aligned beams as analytically determined by using Eq. (6) is compared to the experimental deflection in Fig. 4.

Fig. 5 shows a comparison of the beam deflection during deposition when the reference mismatch strain is, and is not, a function of the out-of-plane coordinate. The solid line indicates the model results when the reference mismatch strain does not vary through

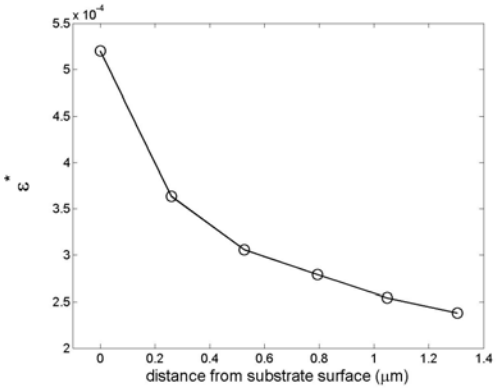

Fig. 3. Reference mismatch strain vs out-of-plane location.

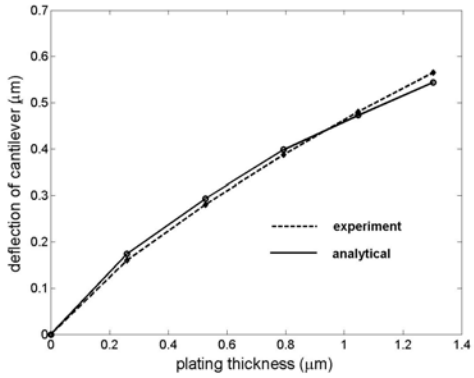

Fig. 4. Beam deflection of the self-assembled cantilevers: analysis and experiment.

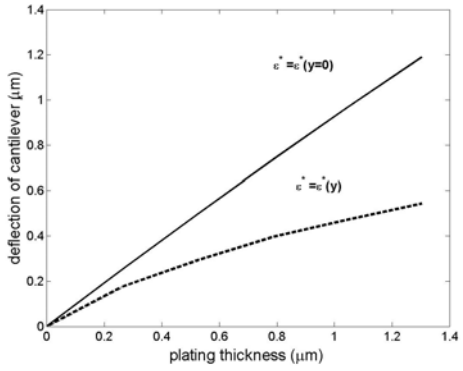

Fig. 5. Comparison of the beam deflection during deposition when the reference mismatch strain is and is not a function of the out-of plane location.

the thickness. These results differ greatly from the real case in which the reference mismatch strain varies through the thickness.

4. Summary

A relation was derived between the mismatch strain, the film thickness, and the displacement of a linear elastic structure under external loading during material deposition. If any two of these variables can be experimentally determined, then the remaining variable can be determined. The method allows one to experimentally determine the mismatch strain by measuring the film thickness and the displacement of a point on the structure that is not undergoing deposition.

A method was presented for using intrinsic (or residual) stresses as a means of self-assembling microstructures during material deposition. The present work extends previous studies because it is assumed herein that the microstructure undergoing deposition is subjected to external loads. Assembly of two components was considered: one component was subjected to deposition and was modeled as an Euler-Bernoulli beam, and the other component did not undergo deposition and was modeled as a linear spring.

The analysis was experimentally verified by electroplating nickel onto an AFM cantilever beam in contact with a second AFM beam (serving as the spring) that did not undergo deposition. The following variables were measured: the stiffness of the spring beam, the dimensions of the deposition beam, the thickness of the various layers that constitute the deposition beam, the Young's modulus of the deposited nickel, and the end deflection of the deposition beam as a function of the deposition thickness when the deposition beam was both attached to and unattached from the spring beam. The mismatch strain was experimentally determined as a function of the deposition thickness. The predicted beam deflection differs greatly depending on whether the reference value of the mismatch strain is assumed to be constant, or whether it varies with the deposition thickness.

Acknowledgments

This research was financially supported by Hansung University in the year of 2007.

References

[1] M. Ataka, A. Omodaka, N. Takeshima and H. Fujita, Fabrication and operation of polyimide bimorph actuators for a ciliary motion system, *Journal of Microelectromechanical Systems* 2 (1993) 146-150.

[2] Y.-P. Ho, M. Wu, H.-Y. Lin and W. Fang, A robust and reliable stress-induced self-assembly mechanism for optical devices, *IEEE/LEOS Int. Conf. on Optical MEMS*, Lugano, Switzerland, (2002) Paper WP38.

[3] H. Xie, Y. Pan and G. K. Fedder, A CMOS-MEMS mirror with curled-hinge comb, *Journal of Microelectromechanical Systems* 12 (2003) 450-457.

[4] V. Y. Prinz, D. Grutzmacher, A. Beyer, C. David, B. Ketterer and E. Deckardt, A new technique for fabricating three-dimensional micro-and nanostructures of various shapes, *Nanotechnology* 12 (2001) 399-402.

[5] B. Mi, D. A. Smith, H. Khan, F. L. Merat, A. H. Heuer and S. M. Phillips, Static and electrically actuated shaped MEMS mirrors, *Journal of Microelectromechanical Systems*, 14 (2005) 29-36.

[6] P. O. Vaccaro, K. Kubota and T. Aida, Strain-driven self-positioning of micromachined structures, *Applied Physics Letters* 78 (2001) 2852-2854.

[7] J. M. Z. Ocampa, P. O. Vaccaro, K. Kubota, T. Fleischmann, T.-S. Wang, T. Aida, T. Ohnishi, A. Sugimura, R. Izumoto, M. Hosoda and S. Nashima, Characterization of GaAs-based micro-origami mirrors by optical actuation, *Microelectronic Engineering* 73-74 (2004) 429-434.

[8] P. O. Vaccaro, K. Kubota, T. Fleischmann, S. Saravann and T. Aida, Valley fold and mountain-fold in the micro-origami technique, *Microelectronics Journals* 34 (2003) 447-449.

[9] A. Vorob'ev, P. O. Vaccaro, K. Kubota, T. Aida, T. Tokuda, T. Hayashi, Y. Sakano, J. Ohta and M. Nunoshita, SiGe/Si microtubes fabricated on a silicon-on-insulator substrate, *Journal of Physics D: Applied Physics* 36 (2003) L71-L73.

[10] M. W. Judy, Y.-H. Cho, R. T. Howe and A. P. Pisano, Self-adjusting microstructures (SAMS), *Tech. Digest, IEEE Micro Electro Mechanical Systems Workshop,* Nara, Japan, (1991) 51-56.

[11] G. G. Stoney, The tension of metallic films deposited by electrolysis, *Proceedings of the Royal Society of London* A82 (1909) 172-175.

[12] L. B. Freund, Some elementary connections be-

tween curvature and mismatch strain in compositionally graded thin films, *Journal of the Mechanics and Physics of Solids* 44 (1996) 723-736.

[13] A. Ni, D. Sherman, R. Ballarini, H. Khan, B. Mi, S. M. Phillips and A. H. Heuer, Optimal design of multilayered polysilicon films for prescribed curvature, *Journal of Materials Science* 38 (2003) 4169-73.

[14] S.-H. Kim and J. G. Boyd, Modeling of mechanical behavior of microcantilever due to intrinsic strain during deposition," *Journal of Mechanical Science and Technology* 20 (2006) 1646-1652.

[15] S.-H. Kim and J. G. Boyd, Analytical and Experimental Study of Mismatch Strain-Induced Microcantilever Behavior during Deposition," *Journal of Mechanical Science and Technology* 21 (2007) 415-420.

[16] J. E. Sader, Calibration of rectangular atomic force microscope cantilever, *Review of Scientific Instruments* 70 (1999) 3967-3969.

[17] W. N. Sharpe, *MEMS Handbook: Chapter 3 – Mechanical Properties of MEMS Material*, CRC Press, Boca Raton, (2002).

[18] M. Schlesinger and M. Paunovic, *Modern Electroplating*, John Wiley & Sons, New York, (2000).

Sang-Hyun Kim obtained his B. S. (1993) and M.S. (1995) degrees in Aerospace Engineering from Pusan Nation University and Ph.D. (2005) in Aerospace Engineering from Texas A&M University. After getting Ph.D., he joined Micro Systems Lab. at Samsung Advanced Institute of Technology (SAIT) and worked in the field of MEMS designs, especially microsensors, microactuator and inkjet print head. He is currently working as a faculty member in Mechanical Systems Engineering at Hansung University. His research interest lies in design, fabrication and test of MEMS/NEMS. He is also interested in the development of design platform of multi-physics and multi-scale phenomena.